applied sciences

MDPI

Article

Performance Prediction of Power Beacon-Aided Wireless Sensor-Powered Non-Orthogonal Multiple-Access Internet-of-Things Networks under Imperfect Channel State Information

Ngoc-Long Nguyen [1], Anh-Tu Le [2], Phuong-Loan T. Nguyen [3], Bui Vu Minh [4,*], Lubos Rejfek [5] and Yong-Hwa Kim [6,*]

1 Faculty of Applied Sciences, Ton Duc Thang University, Ho Chi Minh City 70000, Vietnam; nguyenngoclong@tdtu.edu.vn
2 Faculty of Electrical Engineering and Computer Science, VSB-Technical University of Ostrava, 70800 Ostrava, Czech Republic; tu.le.anh.st@vsb.cz
3 Faculty of Fundamental 2, Posts and Telecommunications Institute of Technology, Ho Chi Minh City 70000, Vietnam; ntploan@ptithcm.edu.vn
4 Faculty of Engineering and Technology, Nguyen Tat Thanh University, Ho Chi Minh City 754000, Vietnam
5 Faculty of Electrical Engineering and Informatics, University of Pardubice, 53210 Pardubice, Czech Republic; lubos.rejfek@upce.cz
6 Department of Artificial Intelligence, Korea National University of Transportation (KNUT), Uiwang-si 16106, Gyeonggi-do, Republic of Korea
* Correspondence: bvminh@ntt.edu.vn (B.V.M.); yongkim@ut.ac.kr (Y.-H.K.)

Abstract: In this paper, we investigate a novel power beacon (PB)-aided wireless sensor-powered non-orthogonal multiple-access (NOMA) Internet-of-Things (IoT) network under imperfect channel state information (CSI). Furthermore, the exact expression outage probability (OP) of two IoT users is derived to analyze the performance of the considered network. To give further insight, the expression asymptotic OP and diversity order are also expressed when the transmit power at the PB goes to infinity. Furthermore, a deep neural network (DNN) framework is proposed to concurrently forecast IoT users' OP in relation to real-time setups for IoT users. Additionally, when compared to the traditional analysis, our created DNN shows the shortest run-time prediction, and the outcomes predicted by the DNN model almost match those of the simulation. In addition, numerical results validate our analysis, simulation, and prediction through a Monte Carlo Simulation. Furthermore, the results show the impact of the main parameter on our proposed system. Finally, these findings show that NOMA performs better than the conventional orthogonal multiple-access (OMA) techniques.

Keywords: IoT; non-orthogonal multiple access (NOMA); imperfect CSI; deep neural network (DNN)

Citation: Nguyen, N.-L.; Le, A.-T.; Nguyen, P.-L.T.; Minh, B.V.; Rejfek, L.; Kim, Y.-H. Performance Prediction of Power Beacon-Aided Wireless Sensor-Powered Non-Orthogonal Multiple-Access Internet-of-Things Networks under Imperfect Channel State Information. *Appl. Sci.* **2024**, *14*, 4498. https://doi.org/10.3390/app14114498

Academic Editor: Alessandro Lo Schiavo

Received: 19 April 2024
Revised: 19 May 2024
Accepted: 21 May 2024
Published: 24 May 2024

1. Introduction

Recently, the Internet of Things (IoTs) has seen significant improvements in machine-to-machine (M2M) interactions, as well as a rising demand for IoT connections. IoT applications use intelligent devices to gather, process, and publish data on a regular basis. Billions of smart devices are connected to the Internet to enable a variety of applications, including smart building, industrial automation, smart health, and smart agriculture. Smart devices can access multimedia devices connected to the Internet of Things [1,2]. Several studies have supported the use of IoT wireless technology. However, it remains difficult to satisfy the demands of IoT applications in the future that will support hundreds of billions of linked devices [3,4]. Non-orthogonal multiple-access (NOMA) approaches are a well-studied strategy for offering significant spectral efficiency (SE) use in IoT networks [5–7], satellite networks [8–10], and V2V networks [11,12]. NOMA enables several users to use the same time and frequency block with varying transmit power allocations [13,14].

Furthermore, it employs superposition coding (SC) on the transmitter to accommodate signals from numerous users, and successive interference cancellation (SIC) at the receiver to separate and decrease interference [15,16]. NOMA technology is critical for future network capacity expansion. In particular, NOMA has been enhanced to increase cooperative communications, allowing users with superior channel conditions to act as a decode-and-forward (DF) or amplify-and-forward (AF) relay, improving information delivery and transmission reliability [17–20]. Moreover, the outage performance of a DF-based NOMA system under full-duplex (FD) and half-duplex (HD) situations was studied in [17]. Furthermore, over Nakagami-*m* fading, the outage probability (OP) and sum rate of the cooperative NOMA system with DF relay were investigated [18]. Additionally, the authors examined the downlink NOMA outage patterns using both DF and AF protocols [19], where it was possible to ascertain the decoding order of cell-edge users' data based on incomplete channel status information. The two-way relay cooperative NOMA system's OP and ergodic rate were studied in light of the possible performance boost provided by FD cooperative NOMA [20].

Wireless power transfer (WPT) is a potential technique for extending the life of energy-constrained wireless networks, such as wireless sensor networks and post-disaster emergency communication [21]. WPT-based networks are classified into two types: simultaneous wireless information and power transfer (SWIPT) [22–24] and wireless-powered communication networks (WPCN) [25–27]. SWIPT transports both information and energy via radio frequency (RF) signals, whereas WPCN harvests energy from a specialized power station and utilizes it for wireless information transmission (WIT) such as a power beacon (PB) or a hybrid access point (HAP). Both models have been thoroughly investigated in a variety of settings, focusing on the trade-off between data rate and energy harvesting (EH) amount with two techniques: the time-switching (TS) and power-splitting (PS) protocols.

Furthermore, the RF-EH protocols for a dual-hop relaying communication system are modeled after the TS and PS SWIPT protocols for non-relay point-to-point networks. In particular, these techniques, called time switching-based relaying (TSR) and power splitting-based relaying (PSR), collect energy from the source information stream [28]. The authors of [29] investigate multiple DF energy-constrained relays utilizing best relay selection and a hybrid TSR/PSR SWIPT RF-EH protocol, calculating OP and ergodic capacity with the extreme value theorem. In [30], the authors investigate a dual-hop cooperative relaying system with numerous energy-constrained relays utilizing the TSR SWIPT RF-EH protocol. The system's OP is calculated using Nakagami-m fading in tight lower limits. In [31], the authors proposed a dual-hop cooperative relaying system with an energy-constrained DF relay that harvests energy from the source information stream. The exact closed-form OP equations are generated using special functions.

Recently, NOMA and cooperative relaying NOMA (C-NOMA) combined with EH have been hotly studied [32–38]. In [32], the authors investigated spatial modulation-based CNOMA for the BS downlink using a full-duplex near user that might collect energy and transmit data to a far user. Ref. [33] investigated collaborative user pairing and resource allocation for WPT-based CNOMA with EH near users. In [34], EH is carried out with CNOMA, and it is taken into consideration by choosing the optimal (decode-and-forward) DF relay. Only a two-user downlink NOMA and the dual-hop scenario are taken into account in the system model and analysis. When there are many EH-based amplify-and-forward (AF) relays between the base station and the far user, the best one can be chosen for data forwarding [35]. In [36], a two-user CNOMA network is explored, with the source node's power consumption lowered to meet the needed transmission rates using both TS relaying and PS relaying strategies. The Lyapunov optimization methodology is utilized by the authors in [37] in order to maximize throughput or restrict transmit power levels. For a wireless-enabled IoT network, the author in [38] proposes a fairness-aware NOMA-based scheduling system. Additionally, they suggest boosting network through throughput-aware NOMA-based scheduling.

Recent research has demonstrated that deep learning (DL) methodologies can help with a variety of real-world challenges in wireless communication networks, such as resource allocation, congestion control, and queue management [39]. In [40], a deep neural network (DNN) was utilized to boost a cell-edge user's productivity under both perfect SIC and imperfect SIC in wireless-powered CR-NOMA-based IoT relay networks. In [41], a DNN was developed to tackle classification and regression issues in cognitive two-way relay networks for a relay. The authors of [42] investigated a DNN incorporated into a NOMA system and achieved outstanding performance in terms of channel encoding, decoding, and detection. Ref. [43] described a unique way to improve service distribution in IoT networks that employed DL to discover the best distribution strategy.

Motivation and Contribution

Due to the benefit of sharing SE and achieving EE through the combination of NOMA and RF-EH, evaluating the performance of integrated systems of IoT networks has become more difficult and has garnered attention in several recent studies. In [44], the authors investigated the optimal sum throughput (STP) of SWIPT IoT relay NOMA systems in relation to the TS factor. The maximum throughput for the PB-assisted EH NOMA multiuser relaying systems across Nakagami-m channels was examined in [45] in order to enhance the NOMA IoT-based system performance. In the meanwhile, with faulty CSI and hardware impairment, the throughput and OP of cooperative PB-assisted EH were studied in [46]. In a recent study, ref. [47] looked into the cooperative multiple PBs' OP for uplink NOMA systems in wirelessly powered IoT applications. However, these works do not consider DNN methods to be able to predict with a low latency and high accuracy, towards practical real-time configurations of C-NOMA IoT networks.

Based on these advantages, we propose a wireless sensor-powered NOMA IoT network under imperfect channel state information (CSI). Furthermore, the PB transmits energy to both the BS and relay to transmit the information. Subsequently, the exact OP is derived to evaluate the outage performance of the proposed network. In particular, we employ the DNN model to predict the performance of the considered system to reduce the complexity of the simulation and calculation. The key differences between our study and previous research are summarized in Table 1. The main contribution of our paper can be summarized as follows:

- We investigate a novel wireless sensor-powered NOMA IoT network, where a PB adopts the TS protocol to transmit the energy to both BS and relaying to transmit information. In particular, the imperfect CSI is considered in the information transmission phase to estimate the complex channel intricacies.
- We analyze the performance in terms of outage probability (OP). To obtain more insight into the considered network, the asymptotic expression OP and diversity order are given. Based on the asymptotic expression OP, we show the main parameters that affect the considered network in high SNR.
- We design the DNN frame to reduce the complexity of the Monte Carlo simulation and the traditional analysis towards practical real-time configurations. The DNN models are demonstrated to be efficient in predicting performance in complicated network scenarios using a low-latency inference technique.

Table 1. Comparison of this work with the reference works

	Our Work	**[44]**	**[45]**	**[46]**	**[47]**	**[48]**	**[49]**
NOMA	✓	✓	✓	✓	✓	✓	✓
Energy harvesting	✓	✓	✓	✓	✓	✓	✓
Imperfect CSI	✓			✓			
Outage probability analysis	✓	✓	✓	✓	✓	✓	✓
Diversity order	✓			✓			
DNN method	✓						

The remainder of this work is organized as follows. Section 2 describes the proposed system model. The performance of the proposed system is given in Section 3. The numerical findings of our suggested system are presented in Section 5. Finally, the conclusion is summarized in Section 6.

2. System Model

This paper considered the power beacon (PB)-aided wireless sensor-powered NOMA IoT networks as in Figure 1, where a base station (S) harvests energy from a PB to transmit the information to two users (an IoT far user (FU) and an IoT near user (NU)) through a DF relay (R). In addition, we assumed that every node had a single antenna and that every node had complete knowledge of the CSI. g_{PS} and g_{PR} are the channel coefficients from PB to S and R, respectively; g_{SR}, g_{RN}, and g_{RF} are the channel coefficients from S to R, R to NU and FU, respectively. Furthermore, all channels follow Rayleigh fading. Thus, $|g_j|^2, j \in \{PS, PR, SR, RN, RF\}$ is an exponential random variable with the probability density function (PDF) and the cumulative distribution function (CDF) expressed, respectively, as

$$f_{|g_j|}(x) = \frac{1}{\Omega_j} e^{-\frac{x}{\Omega_j}} \tag{1}$$

$$F_{|g_j|}(x) = 1 - e^{-\frac{x}{\Omega_j}} \tag{2}$$

where $\Omega_j = d_j^{\ell}$ denotes the average channel gain, d_j denotes the distance, and ℓ denotes the path-loss exponent.

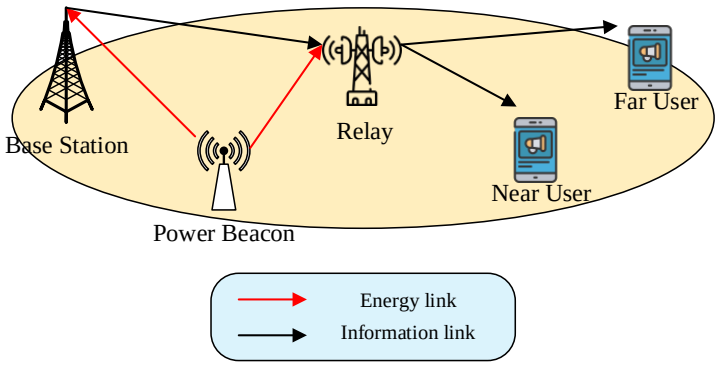

Figure 1. The wireless sensor-powered NOMA IoT network.

Furthermore, we considered the TS protocol for our proposed network as depicted in Figure 2. In particular, the PB transmits the energy to S and R during the period time of βT in the EH phase, where β denotes the TS factor, and T denotes the coherence time block. For the information transmission phase, the remaining time, $(1-\beta)T$, is divided evenly into two hops of transmission, where S and R employ the transmit power derived from the gathered energy for transmitting and relaying operations. Moreover, in the information phase, the channel cannot be perfectly estimated due to the complex channel intricacies. Thus, the channel for the information phase can be modeled as [50]

$$g_z = \varepsilon \hat{g}_z + \sqrt{1-\varepsilon^2}\tilde{g}_z \tag{3}$$

where $z \in \{SR, RN, RF\}$, $\tilde{h}_z$ denotes a circular symmetric complex Gaussian random variable with zero mean and the same variance of h_z, and ε denotes the channel correlation factor that models the accuracy of the channel estimate.

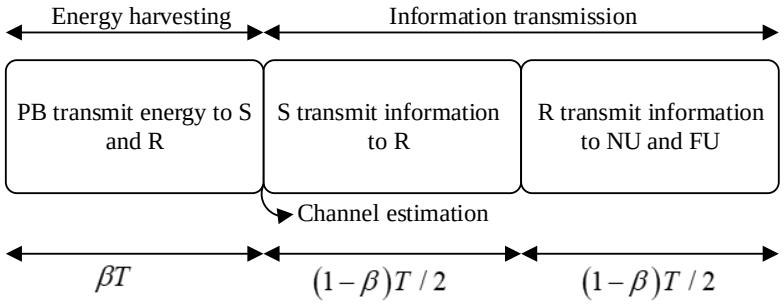

Figure 2. The operational design of the time of the system.

2.1. Energy-Harvesting Phase

In the EH phase, S and R harvest energy from PB during the time period of βT. The total harvested energy at S and R are expressed, respectively, as [48]

$$E_S = \eta\beta T P_{PB}|g_{PS}|^2 \tag{4}$$

$$E_R = \eta\beta T P_{PB}|g_{PR}|^2 \tag{5}$$

where η denotes the energy efficiency, and P_{PB} denotes the transmit power of PB. Furthermore, the transmit power of S and R that was attained in the remaining time $(1-\beta)T/2$ can be given, respectively, as

$$P_S = \frac{E_S}{\frac{(1-\beta)T}{2}} = \frac{2\eta\beta P_{PB}|g_{PS}|^2}{(1-\beta)} = \vartheta P_{PB}|g_{PS}|^2 \tag{6}$$

$$P_R = \frac{E_R}{\frac{(1-\beta)T}{2}} = \frac{2\eta\beta P_{PB}|g_{PR}|^2}{(1-\beta)} = \vartheta P_{PB}|g_{PR}|^2 \tag{7}$$

where $\vartheta = \frac{2\eta\beta}{(1-\beta)}$.

2.2. Information Transmission Phase

In the first information transmission phase, by applying the NOMA protocol, S transmits the superimposed signal $\sqrt{\alpha_N}x_N + \sqrt{\alpha_F}x_F$ to R, where x_N and x_F denotes the signal of NU and FU, respectively, with $\mathbb{E}[|x_N|^2] = \mathbb{E}[|x_F|^2] = 1$; α_N and α_F are the power allocation with $\alpha_N < \alpha_F$ and $\alpha_N + \alpha_F = 1$. Thus, the received signal at R is given by

$$y_R = g_{SR}(\sqrt{\alpha_N}x_N + \sqrt{\alpha_F}x_F)\sqrt{P_S} + n_R \tag{8}$$

where n_R denotes the additive white Gaussian noise with $\mathcal{CN}(0, N_0)$. The signal-to-interference-plus-noise ratios (SINRs) at R when detecting x_F and x_N are given, respectively, as

$$\begin{aligned}\gamma_{R\to x_F} &= \frac{P_S\varepsilon^2\alpha_F|\hat{g}_{SR}|^2}{P_S\alpha_N\varepsilon^2|\hat{g}_{SR}|^2 + P_S(1-\varepsilon^2)\Omega_{SR} + N_0} \\ &= \frac{\vartheta\varepsilon^2\alpha_F|\hat{g}_{SR}|^2|g_{PS}|^2\rho_{PB}}{\alpha_N\varepsilon^2|\hat{g}_{SR}|^2\rho_{PB} + \vartheta(1-\varepsilon^2)\Omega_{SR}|g_{PS}|^2\rho_{PB} + N_0}\end{aligned} \tag{9}$$

$$\gamma_{R\to x_N} = \frac{\vartheta\alpha_N\varepsilon^2\left|\hat{h}_{SR}\right|^2|h_{PS}|^2\rho_{PB}}{\vartheta(1-\varepsilon^2)\Omega_{SR}|h_{PS}|^2\rho_{PB} + 1} \tag{10}$$

where $\rho_{PB} = \frac{P_{PB}}{N_0}$ denotes the average signal-to-noise ratio (SNR).

In the second information transmission phase, R decodes the signal from S and transmits a superimposed signal to two users NU and FU. The received signal at NU and FU are given, respectively, by

$$y_{NU} = g_{RN}(\sqrt{\alpha_N}x_N + \sqrt{\alpha_F}x_F)\sqrt{P_S} + n_{NU} \tag{11}$$

$$y_{NF} = g_{RF}(\sqrt{\alpha_N}x_N + \sqrt{\alpha_F}x_F)\sqrt{P_S} + n_{FU} \tag{12}$$

where n_{NU} and n_{FU} are the AWGN with $\mathcal{CN}(0, N_0)$. The SINR at FU when detecting its own signal x_F is given by

$$\begin{aligned}\gamma_{FU\to x_F} &= \frac{P_R\varepsilon^2\alpha_F|\hat{g}_{FU}|^2}{P_R\alpha_N\varepsilon^2|\hat{g}_{FU}|^2 + P_R(1-\varepsilon^2)\Omega_{FU} + 1} \\ &= \frac{\vartheta\varepsilon^2\alpha_F|g_{PR}|^2|\hat{g}_{FU}|^2\rho_{PB}}{\vartheta\alpha_N\varepsilon^2|g_{PR}|^2|\hat{g}_{FU}|^2\rho_{PB} + \vartheta(1-\varepsilon^2)\Omega_{FU}|g_{PR}|^2\rho_{PB} + 1}\end{aligned} \tag{13}$$

By adopting the SIC process, NU first detects the signal of FU, i.e., x_F, then detects its own signal, i.e., x_n. Thus, the SINRs at NU when detecting signals x_F and x_N are given, respectively, by

$$\gamma_{NU\to x_F} = \frac{\vartheta\varepsilon^2\alpha_F|g_{PR}|^2|\hat{g}_{NU}|^2\rho_{PB}}{\vartheta\alpha_N\varepsilon^2|g_{PR}|^2|\hat{g}_{NU}|^2\rho_{PB} + \vartheta(1-\varepsilon^2)\Omega_{NU}|g_{PR}|^2\rho_{PB} + 1} \tag{14}$$

$$\gamma_{NU\to x_U} = \frac{\vartheta\alpha_N\varepsilon^2|g_{PR}|^2|\hat{g}_{NU}|^2\rho_{PB}}{\vartheta(1-\varepsilon^2)\Omega_{NU}|g_{PR}|^2\rho_{PB} + 1} \tag{15}$$

3. Outage Performance Analysis

3.1. Outage Probability Analysis

The outage event takes place when R and FU cannot properly decode the x_F signal. Therefore, the OP of FU can be determined as

$$P_{FU} = \Pr\left(\min\left(\gamma_{R\to x_F}, \gamma_{FU\to x_F}\right) < \gamma_{FU}\right) \tag{16}$$

where $\gamma_{FU} = 2^{\frac{2R_F}{1-\beta}} - 1$ denotes the threshold, and R_F denotes the target rate.

Theorem 1. *The exact expression OP of FU is expressed as*

$$P_{FU} = 1 - \frac{4\theta_{FU}e^{-2\theta_{FU}\vartheta\left(1-\varepsilon^2\right)\rho_{PB}}}{\sqrt{\Omega_{SR}\Omega_{PS}\Omega_{FU}\Omega_{PR}}}K_1\left(2\sqrt{\frac{\theta_{FU}}{\Omega_{SR}\Omega_{PS}}}\right)K_1\left(2\sqrt{\frac{\theta_{FU}}{\Omega_{FU}\Omega_{PR}}}\right) \tag{17}$$

Proof of Theorem 1. It can be seen in Appendix A. □

The outage event of NU takes place when R and NU cannot properly decode the x_N signal. Thus, the OP of NU can be given by

$$P_{NU} = \Pr\left(\min\left(\gamma_{R\to x_N}, \gamma_{NU\to x_N}\right) < \gamma_{NU}\right) \tag{18}$$

Theorem 2. *The exact expression OP of NU is expressed as*

$$P_{NU} = 1 - \frac{4\theta_{NU}e^{-2\theta_{NU}\vartheta\left(1-\varepsilon^2\right)\rho_{PB}}}{\sqrt{\Omega_{SR}\Omega_{PS}\Omega_{NU}\Omega_{PR}}}K_1\left(2\sqrt{\frac{\theta_{NU}}{\Omega_{SR}\Omega_{PS}}}\right)K_1\left(2\sqrt{\frac{\theta_{NU}}{\Omega_{NU}\Omega_{PR}}}\right) \tag{19}$$

Proof of Theorem 2. With help from (10) and (15), the OP of NU is expressed as

$$P_{NU} = 1 - \Pr\left(|\hat{g}_{SR}|^2 > \left(\vartheta\left(1-\varepsilon^2\right)\Omega_{SR}\theta_{NU}\rho_{PB} + \frac{\theta_{NU}}{|g_{PS}|^2}\right)\right) \times \Pr\left(|\hat{g}_{NU}|^2 > \left(\vartheta\left(1-\varepsilon^2\right)\Omega_{NU}\theta_{NU}\rho_{PB} + \frac{\theta_{NU}}{|g_{PR}|^2}\right)\right) \tag{20}$$

where $\theta_{NU} = \frac{\gamma_{NU}}{\vartheta\varepsilon^2\rho_{PB}\alpha_N}$. Then, the P_{NU} in (20) can be calculated as

$$\begin{aligned} P_{NU} = 1 - &\int_0^\infty f_{|g_{PS}|^2}(x) \int_0^\infty f_{|g_{PR}|^2}(y) \\ &\times F_{|\hat{g}_{SR}|^2}\left(\vartheta\left(1-\varepsilon^2\right)\Omega_{SR}\theta_{NU}\rho_{PB} + \frac{\theta_{NU}}{x}\right)dz \\ &\times F_{|\hat{g}_{NU}|^2}\left(\vartheta\left(1-\varepsilon^2\right)\Omega_{NU}\theta_{NU}\rho_{PB} + \frac{\theta_{NU}}{y}\right)dy \end{aligned} \tag{21}$$

Similarly, in Appendix A, the exact expression OP of NU is given in (19). The proof is completed. □

3.2. Diversity Order Analysis

In this subsection, we express the diversity order to evaluate the OP in high SNRs (i.e., $\rho_{PB} \to \infty$) to obtain more insight into the proposed network. The diversity order is given by [27]

$$d = -\lim_{\rho_{PB}\to\infty} \frac{\log(P^\infty(\rho_{PB}))}{\log(\rho_{PB})} \tag{22}$$

where $P^\infty(\rho_{PB})$ denotes the asymptotic OP of IoT users

Corollary 1. *In high SNR ($\rho_{PB} \to \infty$), we can approximate as $K_1(x) \approx \frac{1}{x}$. Thus, the expression asymptotic OP of FU is expressed as*

$$P_{FU}^\infty \approx 1 - e^{-\frac{2\gamma_{FU}\left(1-\varepsilon^2\right)}{\varepsilon^2(\alpha_F - \gamma_{FU}\alpha_N)}} \tag{23}$$

Remark 1. *Corollary 1 gives some useful insights: (i) the main parameters that affect the OP of FU are the target rate of FU γ_{FU}, the power allocation (α_F, α_N), and the channel correlation factor ε; (ii) upon substituting (23) into (22), the diversity order of FU is zero.*

Corollary 2. *The expression asymptotic OP of NU is expressed as*

$$P_{NU}^\infty \approx 1 - e^{-\frac{2\gamma_{NU}\left(1-\varepsilon^2\right)}{\varepsilon^2\alpha_N}} \tag{24}$$

Remark 2. *Corollary 2 gives some useful insights: (i) the main parameters that affect the OP of NU are the target rate of NU γ_{NU}, the power allocation (α_F, α_N), and the channel correlation factor ε; (ii) upon substituting (24) into (22), the diversity order of FU is zero.*

4. Deep Neural Networks Analysis

In this section, we design and suggest a DNN that can predict the OP in situations where traditional analysis and Monte Carlo simulations are not practical, while having a fast run time and little computing cost. We describe our suggested strategy in more detail below.

4.1. Description of the DNN

Firstly, in order to solve a regression problem, we generated a DNN model. As shown in Figure 3, the DNN model was composed of an input layer, multiple hidden layers, and an output layer. Moreover, in an input layer, we had 15 neurons corresponding to 15 parameters as shown in Table 2. Next, each hidden layer $k = 1, \ldots, D_{hiden}$ had D_{neu} neurons. Furthermore, each hidden neuron employed the rectified linear unit (ReLU) as the nonlinear activation function, defined as [51]

$$ReLU(x) = max(x, 0) \tag{25}$$

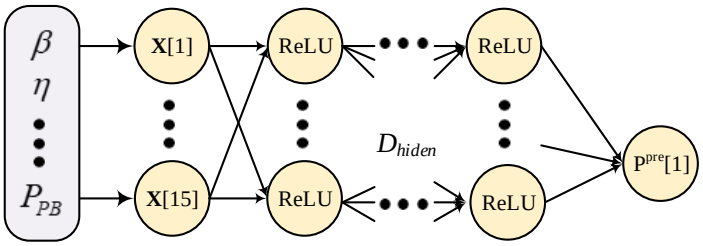

Figure 3. The operational design of DNN for the system.

Table 2. The parameters of the DNN.

Input	Value	Input	Value
β	0.2	d_{SR}	[10,20] [m]
η	0.7	d_{PS}	[10,20] [m]
α_F	0.85	d_{PR}	[10,20] [m]
α_N	0.15	d_{RF}	[20,40] [m]
R_F	[0.01, 0.02]	d_{RN}	[15,30] [m]
R_N	[0.01, 0.02]	N_0	-94 [dBm]
ε	0.95	P_{PB}	[-30,30] [dBm]
ℓ	2.7		

The output layer was composed of a single neuron that utilized the linear activation function to yield the anticipated OP value, $P^{Pre}[1]$. This was because the regression issue sought to estimate an output value without requiring any further conversions.

4.2. Setup for Dataset

In this subsection, each hidden layer k generated the row vector data set $\mathcal{M}$ with data set$[k] = [\mathbf{X}[k], P^{Sim}]$, where $\mathbf{X}[k]$ denotes the feature vector made up of all inputs from each of the parameters in Table 2. Next, the real-value OP sets from (16) and (18) were generated using each $\mathbf{X}[k]$ feature vector, which were then input into the simulation to obtain a distinct matching P^{Sim}. In summary, the data set was created by concatenating the 10^5 samples and was then separated into three new data sets: 80% for training ($\mathcal{M}_{train}$), 10% for validation ($\mathcal{M}_{vali}$), and 10% for testing ($\mathcal{M}_{test}$).

The mean squared error (MSE), defined as $MSE = \frac{1}{\mathcal{M}_{test}} \sum_{k=0}^{\mathcal{M}_{test}-1} (P^{Pre} - P^{sim})$, was used to assess how effectively the suggested DL approach performed. To calculate the difference between the natural and predicted OP values for the full test set, we use the root-mean-square error (RMSE) in the OP prediction, and it can be defined as $RMSE = \sqrt{MSE}$.

5. Numerical Result

In this section, we provide illustrative numerical results to evaluate the performance of the proposed network in terms of OP by using a Monte Carlo simulation. The main parameters were set as $\beta = 0.2$, $d_{SR} = 10$ m, $\eta = 0.7$, $d_{PS} = 10$ m, $\alpha_F = 0.85$, $d_{PR} = 10$ m, $\alpha_N = 0.15$, $d_{RF} = 20$ m, $d_{RN} = 15$ m, $R_N = 0.01$, $R_F = 0.01$, $N_0 = -94$ [dBm], $\varepsilon = 0.95$,

and $\ell = 2.7$, except for the special case. Furthermore, Ana., Sim., and Asymp. are the abbreviations for analytical, simulation, and asymptotic, respectively. For the DNN, we set five hidden layers with each layer having 128 neurons, which was implemented in Python 3.11.4 using Keras 2.8.0 and TensorFlow 2.8.0, with 100 epochs for training the DNN.

In Figure 4, we utilized the MSE of the training and the validation to evaluate the accuracy of the proposed DNN. As can be seen, the MSE converged to a value lower than 10^{-5} after 40 epochs. Figure 5 plots the OP of two users (FU and NU) versus P_{PB} in dBm while varying the target rate $R_F = R_N$. It can be observed that over the whole range of P_{PB} in dBm, the OP curves and analytical results agreed exceptionally well based on the Monte Carlo simulation. Furthermore, the asymptotic findings produced in (23) and (24) were extremely valid with the theoretical analysis ones at high P_{PB}, confirming the accuracy of our developed analysis approach. In addition, we can observe that the outage performance was improved when increasing the transmit power but did not change in high P_{PB}. The fact that the OP depended on more factors than only transmitting P_{PB} can be shown in Remark 1 and 2. Another observation is that the excellent agreement between the simulation and DNN prediction outcomes validated our proposed methods.

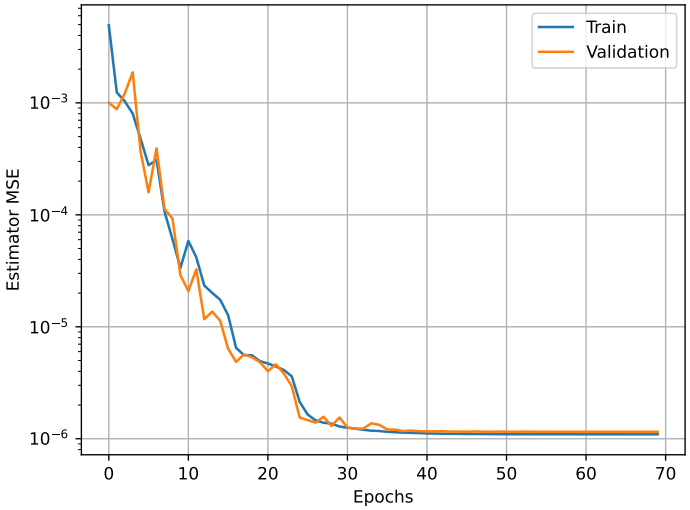

Figure 4. The MSE for DNN training and validation .

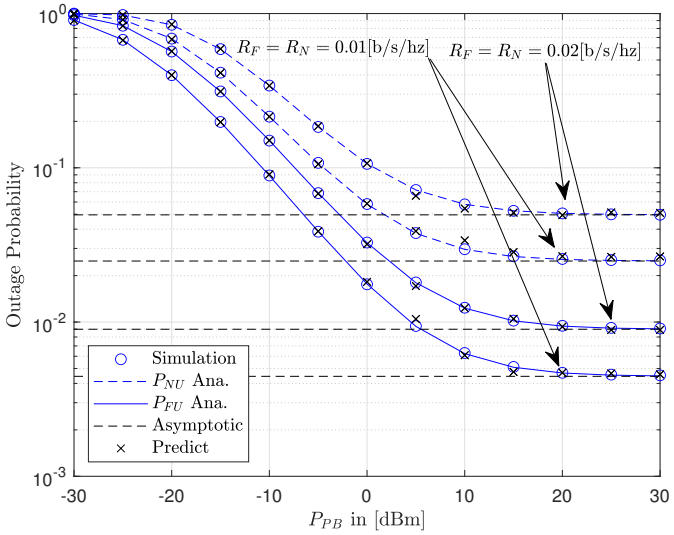

Figure 5. The outage probability versus P_{PB} in dBm when varying the target rate $R_F = R_N$.

Figure 6 depicts the OP of users versus P_{PB} in dBm with varying ε. As shown in Figure 6, we can observe that the OP increased when β decreased and converge with a large P_{PB}. This is due to the OP depending on the interference channels in the SINR of two users when decoding the signal. In Figure 7, we plotted the OP versus α_F when varying P_{PB} in dBm. First, we can observe that the OP of FU decreased when α_F increased. The reason was that when α_F increased, the transmit power of FU was greater than that of NU. Furthermore, the OP of NOMA was better that OMA in the range $0.5 < \beta < 0.8$. In addition, there existed an optimal point α_F for the OP of two users. Specifically, when $P_{PB} = -10$ dBm the optimal point for the OP of two users was $\alpha_F = 0.64$, $\alpha_F = 0.59$ for $P_{PB} = 0$ dBm, and $\alpha_F = 0.54$ for $P_{PB} = 10$ dBm.

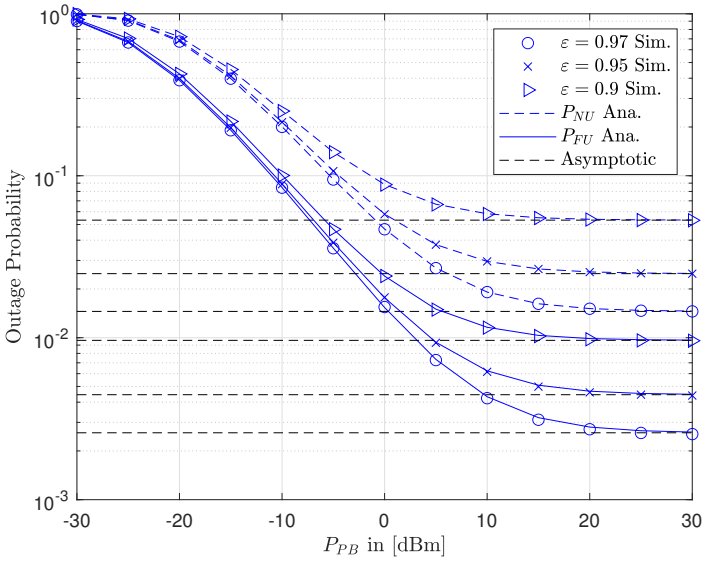

Figure 6. The outage probability versus P_{PB} in dBm when varying ε.

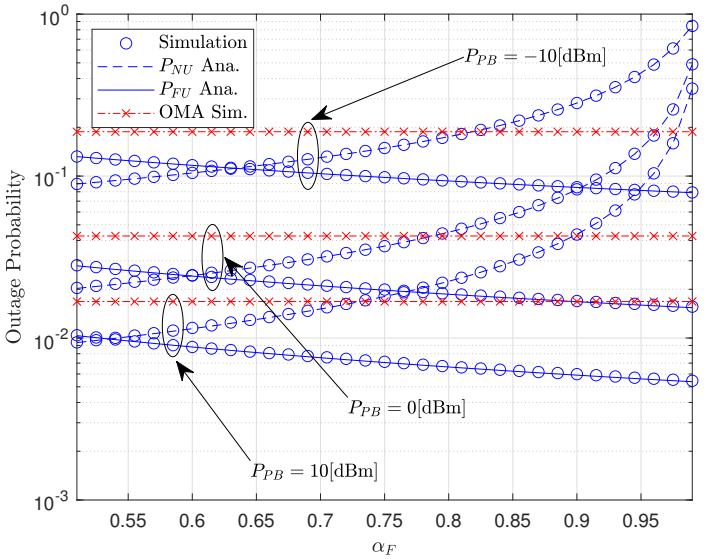

Figure 7. The outage probability versus α_F when varying P_{PB} dBm.

Figure 8 shows the OP of two users versus η when varying P_{PB}. It can be observed that the OP was improved when increasing the energy efficiency η. This is due to the energy efficiency η being larger, leading to a greater transmit power of PB in (4) and (5). Figure 9 illustrates the OP of two users versus β when varying P_{PB}. The TS factor β is important because it controls both the data transport and the amount of energy collected at S and

R. We can observe that the best OP for two users for $P_{PB} = 0$ dBm can be achieved when $0.4 < \beta < 0.5$, and for $P_{PB} = 10$ dBm, the best OP can be achieved when $0.1 < \beta < 0.2$.

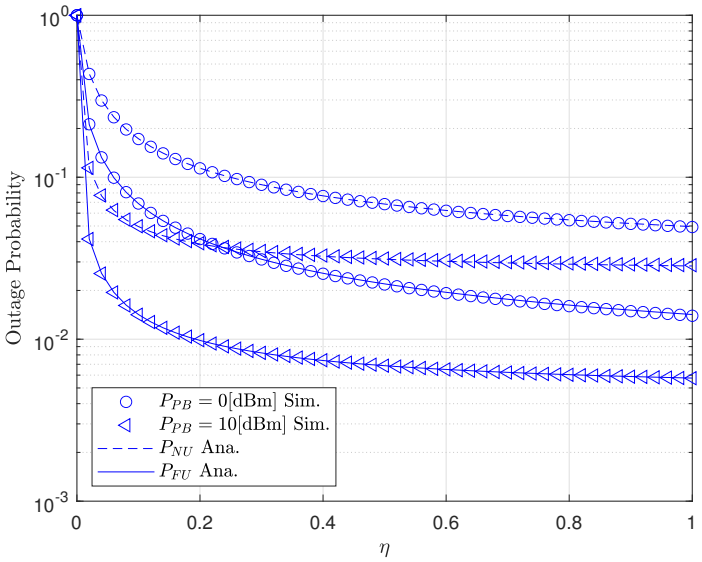

Figure 8. The outage probability versus η when varying P_{PB}.

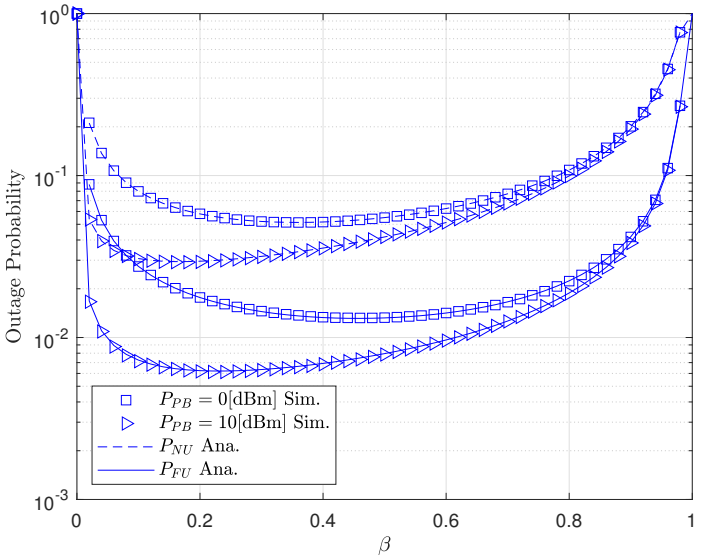

Figure 9. The outage probability versus β when varying P_{PB}.

6. Conclusions

This paper investigated the PB-aided wireless sensor-powered NOMA IoT networks under imperfect CSI. The exact expression OP, expression asymptotic OP, and diversity order were derived to obtain more insight into the system characteristics. Based on the expression asymptotic OP, we showed the main parameter that affected the proposed network such as the channel correlation factor, the power allocation, the factor of TS, and the target rate of users. A DNN was developed to predict the performance in terms of OP with minimal complexity and high accuracy. In the numerical result, this paper found that using a DNN model for system performance evaluation, the OP outcomes closely resembled the Monte Carlo simulation and analysis results.

Author Contributions: N.-L.N. proposed the system model and idea. A.-T.L. and P.-L.T.N. derived the expressions to examine the system performance. B.V.M. and L.R. double-checked the manuscript and simulated the figures. N.-L.N. and Y.-H.K. wrote the whole paper. All authors have read and agreed to the published version of the manuscript.

Funding: This work was supported in part by the National Research Foundation of Korea (NRF) grant funded by the Korea government (MSIT) (No. 2022R1F1A1074975) and in part by the Korea Institute of Energy Technology Evaluation and Planning (KETEP) and the Ministry of Trade, Industry and Energy (MOTIE) of the Republic of Korea (No. 20221A10100011).

Institutional Review Board Statement: Not applicable.

Informed Consent Statement: Not applicable.

Data Availability Statement: Data is contained within the article.

Conflicts of Interest: The authors declare no conflicts of interest.

Appendix A

Proof of Theorem 1. From (9) and (13), the OP of FU can be rewritten as

$$P_{FU} = 1 - \Pr\left(|\hat{g}_{SR}|^2 > \left(\vartheta\left(1-\varepsilon^2\right)\Omega_{SR}\theta_{FU}\rho_{PB} + \frac{\theta_{FU}}{|g_{PS}|^2}\right)\right) \times \Pr\left(|\hat{g}_{FU}|^2 > \left(\vartheta\left(1-\varepsilon^2\right)\Omega_{FU}\theta_{FU}\rho_{PB} + \frac{\theta_{FU}}{|g_{PR}|^2}\right)\right) \tag{A1}$$

where $\theta_{FU} = \frac{\gamma_{FU}}{\vartheta\varepsilon^2\rho_{PB}(\alpha_F - \gamma_{FU}\alpha_N)}$. Next, P_{FU} can be calculated as

$$P_{FU} = 1 - \int_0^\infty f_{|g_{PS}|^2}(x) \int_0^\infty f_{|g_{PR}|^2}(y) \times F_{|\hat{g}_{SR}|^2}\left(\theta_{FU}\vartheta\left(1-\varepsilon^2\right)\Omega_{SR}\rho_{PB} + \frac{\theta_{FU}}{x}\right)dz \times F_{|\hat{g}_{FU}|^2}\left(\theta_{FU}\vartheta\left(1-\varepsilon^2\right)\Omega_{FU}\rho_{PB} + \frac{\theta_{FU}}{y}\right)dy \tag{A2}$$

With (1), (2) and Eq. (3.471.4) from [52] , we obtain

$$\begin{aligned} P_{FU} &= 1 - \frac{e^{-2\theta_{FU}\vartheta\left(1-\varepsilon^2\right)\rho_{PB}}}{\Omega_{PS}\Omega_{PR}} \int_0^\infty e^{-\frac{x}{\Omega_{PS}}} e^{-\frac{\theta_{FU}}{\Omega_{SR}x}} dz \int_0^\infty e^{-\frac{y}{\Omega_{PR}}} e^{-\frac{\theta_{FU}}{\Omega_{FU}y}} dy \\ &= 1 - \frac{4e^{-2\theta_{FU}\vartheta\left(1-\varepsilon^2\right)\rho_{PB}}\theta_{FU}}{\sqrt{\Omega_{SR}\Omega_{PS}\Omega_{FU}\Omega_{PR}}} K_1\left(2\sqrt{\frac{\theta_{FU}}{\Omega_{SR}\Omega_{PS}}}\right) K_1\left(2\sqrt{\frac{\theta_{FU}}{\Omega_{FU}\Omega_{PR}}}\right) \end{aligned} \tag{A3}$$

where K_v denotes the v-order modified Bessel function of the second kind. The proof is completed. □

References

1. Guo, F.; Yu, F.R.; Zhang, H.; Li, X.; Ji, H.; Leung, V.C.M. Enabling Massive IoT Toward 6G: A Comprehensive Survey. *IEEE Internet Things J.* **2021**, *8*, 11891–11915. [CrossRef]
2. Suo, H.; Wan, J.; Zou, C.; Liu, J. Security in the Internet of Things: A Review. In Proceedings of the 2012 International Conference on Computer Science and Electronics Engineering, Hangzhou, China, 23–25 March 2012 ; Volume 3, pp. 648–651. [CrossRef]
3. Vu, T.H.; Nguyen, T.V.; Nguyen, T.T.; Kim, S. Performance Analysis and Deep Learning Design of Wireless Powered Cognitive NOMA IoT Short-Packet Communications With Imperfect CSI and SIC. *IEEE Internet Things J.* **2022**, *9*, 10464–10479. [CrossRef]
4. Nguyen, H.; Nguyen, T.N.; Minh, B.V.; Pham, T.H.T.; Le, A.T.; Voznak, M. Security-Reliability Analysis in CR-NOMA IoT Network Under I/Q Imbalance. *IEEE Access* **2023**, *11*, 119045–119056. [CrossRef]

5. Ghosh, S.; Al-Dweik, A.; Alouini, M.S. On the Performance of End-to-End Cooperative NOMA-Based IoT Networks With Wireless Energy Harvesting. *IEEE Internet Things J.* **2023**, *10*, 16253–16270. [CrossRef]
6. Le, S.P.; Nguyen, H.N.; Nguyen, N.T.; Van, C.H.; Le, A.T.; Voznak, M. Physical layer security analysis of IRS-based downlink and uplink NOMA networks. *Eurasip J. Wirel. Commun. Netw.* **2023**, *2023*, 105. [CrossRef]
7. Le, A.T.; Hieu, T.D.; Nguyen, T.N.; Le, T.L.; Nguyen, S.Q.; Voznak, M. Physical layer security analysis for RIS-aided NOMA systems with non-colluding eavesdroppers. *Comput. Commun.* **2024**, *219*, 194–203. [CrossRef]
8. Le, A.T.; Ha, N.D.X.; Do, D.T.; Yadav, S.; Lee, B.M. Enabling NOMA in Overlay Spectrum Sharing in Hybrid Satellite-Terrestrial Systems. *IEEE Access* **2021**, *9*, 56616–56629. [CrossRef]
9. Nguyen, N.T.; Nguyen, H.N.; Nguyen, N.L.; Le, A.T.; Nguyen, T.N.; Voznak, M. Performance Analysis of NOMA-Based Hybrid Satellite-Terrestrial Relay System Using mmWave Technology. *IEEE Access* **2023**, *11*, 10696–10707. [CrossRef]
10. Chen, B.; Xu, D. Outage Performance of Overlay Cognitive Satellite-Terrestrial Networks With Cooperative NOMA. *IEEE Syst. J.* **2024**, *18*, 222–233. [CrossRef]
11. Jaiswal, N.; Purohit, N. Performance Analysis of NOMA-Enabled Vehicular Communication Systems With Transmit Antenna Selection Over Double Nakagami-m Fading. *IEEE Trans. Veh. Technol.* **2021**, *70*, 12725–12741. [CrossRef]
12. Hieu, T.C.; Cuong, N.L.; Nguyen, B.C.; Hiep, P.T. Full-duplex protocol for vehicle-to-vehicle NOMA relay system over double Rayleigh fading. *Telecommun. Syst.* **2022**, *80*, 337–347. [CrossRef]
13. Do, D.T.; Le, A.T.; Lee, B.M. NOMA in Cooperative Underlay Cognitive Radio Networks Under Imperfect SIC. *IEEE Access* **2020**, *8*, 86180–86195. [CrossRef]
14. Mlika, Z.; Cherkaoui, S. Massive IoT Access With NOMA in 5G Networks and Beyond Using Online Competitiveness and Learning. *IEEE Internet Things J.* **2021**, *8*, 13624–13639. [CrossRef]
15. Ding, Z.; Liu, Y.; Choi, J.; Sun, Q.; Elkashlan, M.; Chih-Lin, I.; Poor, H.V. Application of Non-Orthogonal Multiple Access in LTE and 5G Networks. *IEEE Commun. Mag.* **2017**, *55*, 185–191. [CrossRef]
16. Sirait, R.; Hardjawana, W.; Wibisono, G. Performance of Downlink NOMA for a Massive IoT Network Over a Nakagami-m Fading Channel With Optimized Power Allocation. *IEEE Access* **2023**, *11*, 67779–67790. [CrossRef]
17. Yue, X.; Liu, Y.; Kang, S.; Nallanathan, A.; Ding, Z. Exploiting Full/Half-Duplex User Relaying in NOMA Systems. *IEEE Trans. Commun.* **2018**, *66*, 560–575. [CrossRef]
18. Chu, T.M.C.; Zepernick, H.J. Performance of a Non-Orthogonal Multiple Access System With Full-Duplex Relaying. *IEEE Commun. Lett.* **2018**, *22*, 2084–2087. [CrossRef]
19. Wan, D.; Wen, M.; Ji, F.; Liu, Y.; Huang, Y. Cooperative NOMA Systems With Partial Channel State Information Over Nakagami-*m* Fading Channels. *IEEE Trans. Commun.* **2018**, *66*, 947–958. [CrossRef]
20. Wang, X.; Jia, M.; Ho, I.W.H.; Guo, Q.; Lau, F.C.M. Exploiting Full-Duplex Two-Way Relay Cooperative Non-Orthogonal Multiple Access. *IEEE Trans. Commun.* **2019**, *67*, 2716–2729. [CrossRef]
21. Zhao, N.; Lu, W.; Sheng, M.; Chen, Y.; Tang, J.; Yu, F.R.; Wong, K.K. UAV-Assisted Emergency Networks in Disasters. *IEEE Wirel. Commun.* **2019**, *26*, 45–51. [CrossRef]
22. Zhang, X.; Wang, J.; Poor, H.V. Statistical Delay and Error-Rate Bounded QoS Provisioning for SWIPT Over CF M-MIMO 6G Mobile Wireless Networks Using FBC. *IEEE J. Sel. Top. Signal Process.* **2021**, *15*, 1272–1287. [CrossRef]
23. Tin, P.T.; Nguyen, T.N.; Tran, D.H.; Voznak, M.; Phan, V.D.; Chatzinotas, S. Performance enhancement for full-duplex relaying with time-switching-based SWIPT in wireless sensors networks. *Sensors* **2021**, *21*, 3847. [CrossRef]
24. Nguyen, T.N.; Tran, D.H.; Van Chien, T.; Phan, V.D.; Voznak, M.; Chatzinotas, S. Security and Reliability Analysis of Satellite-Terrestrial Multirelay Networks With Imperfect CSI. *IEEE Syst. J.* **2023**, *17*, 2824–2835. [CrossRef]
25. Huang, K.; Lau, V.K.N. Enabling Wireless Power Transfer in Cellular Networks: Architecture, Modeling and Deployment. *IEEE Trans. Wirel. Commun.* **2014**, *13*, 902–912. [CrossRef]
26. Nguyen, B.C.; Hoang, T.M.; Tran, P.T.; Nguyen, T.N. Outage probability of NOMA system with wireless power transfer at source and full-duplex relay. *AEU-Int. J. Electron. Commun.* **2020**, *116*, 152957. [CrossRef]
27. Le, A.T.; Tran, D.H.; Le, C.B.; Tin, P.T.; Nguyen, T.N.; Ding, Z.; Poor, H.V.; Voznak, M. Power Beacon and NOMA-Assisted Cooperative IoT Networks With Co-Channel Interference: Performance Analysis and Deep Learning Evaluation. *IEEE Trans. Mob. Comput.* **2023**, *23*, 7270–7283 . [CrossRef]
28. Nasir, A.A.; Zhou, X.; Durrani, S.; Kennedy, R.A. Relaying Protocols for Wireless Energy Harvesting and Information Processing. *IEEE Trans. Wirel. Commun.* **2013**, *12*, 3622–3636. [CrossRef]
29. Subhash, A.; Kalyani, S. Cooperative Relaying in a SWIPT Network: Asymptotic Analysis Using Extreme Value Theory for Non-Identically Distributed RVs. *IEEE Trans. Commun.* **2021**, *69*, 4360–4372. [CrossRef]
30. Hoang, T.M.; Nguyen, B.C.; Tran, P.T.; Dung, L.T. Outage Analysis of RF Energy Harvesting Cooperative Communication Systems Over Nakagami-*m* Fading Channels With Integer and Non-Integer *m*. *IEEE Trans. Veh. Technol.* **2020**, *69*, 2785–2801. [CrossRef]
31. Do, T.N.; da Costa, D.B.; Duong, T.Q.; An, B. Improving the Performance of Cell-Edge Users in MISO-NOMA Systems Using TAS and SWIPT-Based Cooperative Transmissions. *IEEE Trans. Green Commun. Netw.* **2018**, *2*, 49–62. [CrossRef]
32. Si, Q.; Jin, M.; Tsiftsis, T.A.; Zhao, N.; Wang, X. Cooperative SM-Based NOMA Scheme With SWIPT. *IEEE Trans. Veh. Technol.* **2021**, *70*, 6195–6199. [CrossRef]

33. Wu, M.; Song, Q.; Guo, L.; Jamalipour, A. Joint User Pairing and Resource Allocation in a SWIPT-Enabled Cooperative NOMA System. *IEEE Trans. Veh. Technol.* **2021**, *70*, 6826–6840. [CrossRef]
34. Rauniyar, A.; Engelstad, P.; Østerb, O.N. RF Energy Harvesting and Information Transmission Based on Power Splitting and NOMA for IoT Relay Systems. In Proceedings of the 2018 IEEE 17th International Symposium on Network Computing and Applications (NCA), Cambridge, MA, USA, 1–3 November 2018; pp. 1–8. [CrossRef]
35. Li, X.; Wang, Q.; Liu, M.; Li, J.; Peng, H.; Piran, M.J.; Li, L. Cooperative Wireless-Powered NOMA Relaying for B5G IoT Networks With Hardware Impairments and Channel Estimation Errors. *IEEE Internet Things J.* **2021**, *8*, 5453–5467. [CrossRef]
36. Lan, X.; Zhang, Y.; Chen, Q.; Cai, L. Energy Efficient Buffer-Aided Transmission Scheme in Wireless Powered Cooperative NOMA Relay Network. *IEEE Trans. Commun.* **2020**, *68*, 1432–1447. [CrossRef]
37. Ren, J.; Lei, X.; Zhou, F.; Diamantoulakis, P.D.; Dobre, O.A.; Karagiannidis, G.K. Throughput Maximization in Buffer-aided Wireless-Powered NOMA Networks. In Proceedings of the ICC 2020–2020 IEEE International Conference on Communications (ICC), Dublin, Ireland, 7–11 June 2020; pp. 1–7. [CrossRef]
38. Liu, Y.; Chen, X.; Cai, L.X.; Chen, Q.; Zhang, R. Nonorthogonal Multiple Access for Wireless-Powered IoT Networks. *IEEE Internet Things J.* **2021**, *8*, 112–128. [CrossRef]
39. Huang, H.; Guo, S.; Gui, G.; Yang, Z.; Zhang, J.; Sari, H.; Adachi, F. Deep Learning for Physical-Layer 5G Wireless Techniques: Opportunities, Challenges and Solutions. *IEEE Wirel. Commun.* **2020**, *27*, 214–222. [CrossRef]
40. Vu, T.H.; Nguyen, T.V.; Kim, S. Wireless Powered Cognitive NOMA-Based IoT Relay Networks: Performance Analysis and Deep Learning Evaluation. *IEEE Internet Things J.* **2022**, *9*, 3913–3929. [CrossRef]
41. Zhang, Z.; Lu, Y.; Huang, Y.; Zhang, P. Neural Network-Based Relay Selection in Two-Way SWIPT-Enabled Cognitive Radio Networks. *IEEE Trans. Veh. Technol.* **2020**, *69*, 6264–6274. [CrossRef]
42. Gui, G.; Huang, H.; Song, Y.; Sari, H. Deep Learning for an Effective Nonorthogonal Multiple Access Scheme. *IEEE Trans. Veh. Technol.* **2018**, *67*, 8440–8450. [CrossRef]
43. Manogaran, G.; Nguyen, T.N.; Gao, J.; Kumar, P.M. Deep Learning-Based Service Distribution Model for Wireless Network Assisted Internet of Everything. *IEEE Trans. Netw. Sci. Eng.* **2022**, *9*, 3004–3014. [CrossRef]
44. Rauniyar, A.; Engelstad, P.; Østerbø, O.N. RF Energy Harvesting and Information Transmission in IoT Relay Systems based on Time Switching and NOMA. In Proceedings of the 2018 28th International Telecommunication Networks and Applications Conference (ITNAC), Sydney, Australia, 21–23 November 2018; pp. 1–7. [CrossRef]
45. Hoang, T.M.; Tan, N.T.; Tran, X.N. Performance analysis of power beacon-assisted energy harvesting NOMA multi-user relaying system over Nakagami-m fading channels. *AEU-Int. J. Electron. Commun.* **2020**, *115*, 153022. [CrossRef]
46. Li, X.; Liu, M.; Deng, D.; Li, J.; Deng, C.; Yu, Q. Power beacon assisted wireless power cooperative relaying using NOMA with hardware impairments and imperfect CSI. *AEU-Int. J. Electron. Commun.* **2019**, *108*, 275–286. [CrossRef]
47. Do, D.T.; Nguyen, M.S.V.; Nguyen, T.N.; Li, X.; Choi, K. Enabling Multiple Power Beacons for Uplink of NOMA-Enabled Mobile Edge Computing in Wirelessly Powered IoT. *IEEE Access* **2020**, *8*, 148892–148905. [CrossRef]
48. Vu, T.H.; Kim, S. Performance Evaluation of Power-Beacon-Assisted Wireless-Powered NOMA IoT-Based Systems. *IEEE Internet Things J.* **2021**, *8*, 11655–11665. [CrossRef]
49. Zhang, Y.; Feng, S.; Tang, W. Performance Analysis and Optimization for Power Beacon-Assisted Wireless Powered Cooperative NOMA Systems. *IEEE Access* **2020**, *8*, 198436–198450. [CrossRef]
50. Vu, T.H.; Kim, S. Performance Analysis of Full-Duplex Two-Way RIS-Based Systems With Imperfect CSI and Discrete Phase-Shift Design. *IEEE Commun. Lett.* **2023**, *27*, 512–516. [CrossRef]
51. Nwankpa, C.; Ijomah, W.; Gachagan, A.; Marshall, S. Activation functions: Comparison of trends in practice and research for deep learning. *arXiv* **2018**, arXiv:1811.03378.
52. Gradshteyn, I.S.; Ryzhik, I.M. *Table of Integrals, Series, and Products*; Academic Press: Cambridge, MA, USA, 2014.